Published in final edited form as:
Inorg Chem. 2010 July 5; 49(13): 5963–5970. doi:10.1021/ic1004616.

Activation of a PARACEST Agent for MRI through Selective Outersphere Interactions with Phosphate Diesters

Ching-Hui Huang[1], **Jacob Hammell**[1], **S. James Ratnakar**[2], **A. Dean Sherry**[2,3], and **Janet R. Morrow**[1]

Ching-Hui Huang: ch52@buffalo.edu; A. Dean Sherry: sherry@utdallas.edu; Janet R. Morrow: Jmorrow@buffalo.edu

[1]Department of Chemistry, University at Buffalo, State University of New York, Buffalo, NY 14260, Fax (1)716-645-6963

[2]Advanced Imaging Research Center, University of Texas Southwestern Medical Center, 2201 Inwood Road, Dallas, TX 75390-8568

[3]Department of Chemistry, University of Texas, Dallas, P.O. Box 830688, Richardon, TX 75083-0688, Fax (1) 972-883-2025

Abstract

Ln(**S-THP**)$^{3+}$ complexes are paramagnetic chemical exchange saturation transfer agents (PARACEST) agents for magnetic resonance imaging (MRI) (**S-THP** = (1S,4S,7S,10S)-1,4,7,10-tetrakis(2-hydroxypropyl)-1,4,7,10-tetraazacyclododecane, Ln(III) = Ce(III), Eu(III), Yb(III)). CEST spectra at 11.7 T show that the PARACEST effect of these complexes is enhanced at neutral pH in buffered solutions containing 100 mM NaCl upon addition of 1–2 equivalents of diethylphosphate (**DEP**). CEST images of phantoms at 4.7 T confirm that **DEP** enhances the properties of Yb(**S-THP**)$^{3+}$ as a PARACEST MRI agent in buffered solutions at neutral pH and 100 mM NaCl. Studies using ^{1}H NMR, direct excitation Eu(III) luminescence spectroscopy, and UV-visible spectroscopy show that **DEP** is an outersphere ligand. Dissociation constants for [Ln(**S-THP**)(OH_2)](**DEP**) are 1.9 mM and 2.8 mM for Ln(III) = Yb(III) at pH 7.0 and Eu(III) at pH 7.4, respectively. Related ligands including phosphorothioic acid, O,O-diethylester, ethyl methylphosphonate, O-(4-nitrophenylphosphoryl)choline and cyclic 3,5-adenosine monophosphate do not activate PARACEST. **BNPP** (bis(4-nitrophenyl phosphate) activates PARACEST of Ln(**S-THP**)$^{3+}$ (Ln(III) = Eu(III), Yb(III)), albeit less effectively than does **DEP**. This data shows that binding through second coordination sphere interactions is selective for phosphate diesters with two terminal oxygens and two identical ester groups. A crystal structure of [Eu(**S-THP**)(OH_2)]((O_2NPhO)$_2$$PO_2$)$_2$($CF_3SO_3$) · 2$H_2O$ · iPrOH has two outersphere **BNPP** anions that form hydrogen bonds to the alcohol groups of the macrocycle and the bound water ligand. This structure supports ^{1}H NMR spectroscopy studies showing that outersphere interactions of the phosphate diester with the alcohol protons modulate the rate of alcohol proton exchange to influence the PARACEST properties of the complex. Further, **DEP** interacts only with the non-ionized form of the complex, Ln(**S-THP**)(OH_2)$^{3+}$ contributing to the pH dependence of the PARACEST effect.

Correspondence to: Janet R. Morrow, Jmorrow@buffalo.edu.

Supporting Information Available: Listings of CEST, ^{1}H NMR and luminescence spectra. This material is available free of charge via the Internet at http://pubs.acs.org

Introduction

The development of Ln(III) magnetic resonance imaging (MRI) contrast agents that report on their environment through molecular interactions is an active area of research.[1–3] Ln(III) MRI agents have been designed for sensing pH,[4] metabolite concentrations,[5–7] metal ions, [8–10] proteins,[11] or enzymes.[12–13] Both innersphere and outersphere interactions induce changes in the properties of MRI contrast agents. For the well-known Gd(III) MRI contrast agents, contrast properties are modulated through a change in the number of exchangeable water ligands in the inner coordination sphere[3] or through an change in rotational correlation time and associated relaxivity induced by binding to a macromolecule.[14] To a lesser extent, outersphere anions or cations may serve to modulate the water structure around the Gd(III) cation with the net effect of influencing water ligand exchange, an important property for this class of MRI contrast agent.[15–18]

A relatively new class of contrast agent known as paramagnetic chemical exchange saturation transfer (PARACEST) agents, shows promise for development as responsive MRI agents.[19] PARACEST agents are paramagnetic Ln(III) complexes that have mobile protons in chemical exchange with bulk water.[20–21] Application of a presaturation pulse at the resonance frequency of the mobile protons leads to a reduction of the bulk water proton resonance through exchange of the saturated lanthanide complex protons with bulk water. Efforts have been made to develop PARACEST agents that respond to both outer and innersphere ligands. Macrocyclic Ln(III) complexes have been functionalized to bind Zn(II) or neutral small molecules such as glucose in remote binding pockets.[22–23] The PARACEST spectrum of these complexes changes due to outersphere water-mediated interactions that influence the mobile protons of the water ligand. Metabolites that act as innersphere ligands also modulate the PARACEST effect of Ln(III) complexes, generally by changing the chemical shift of the mobile proton resonance that gives rise to the PARACEST effect.[24–25] A variation of this theme is found in the PARACEST agents that are activated by enzymatic cleavage of pendent groups to create a new innersphere donor group with exchangeable protons.[12–13]

Ln(**S-THP**)$^{3+}$ complexes (Ln = Ce(III), Eu(III), Yb(III)) act as responsive PARACEST agents for magnetic resonance imaging (Chart 1) through exchange of the alcohol protons of the macrocyclic complex.[24,26–27] Changes in PARACEST properties of these complexes are affected by both outersphere and innersphere ligand interactions.[24] Notably, the PARACEST properties of these complexes are not optimal under physiological conditions of neutral pH, but are highly pH dependent over the pH range of 3–7. Optimal conditions for chemical exchange saturation transfer (CEST) of the alcohol protons are observed at pH 3 for Yb(**S-THP**)$^{3+}$, pH 5 for Eu(**S-THP**)$^{3+}$ and pH 6 for Ce(**S-THP**)$^{3+}$. [26] We previously showed that addition of diethylphosphate (**DEP**) modulates the PARACEST effect for Eu(**S-THP**)$^{3+}$ at near neutral pH through an outersphere interaction. In the present work, we seek to understand the mechanism for modulation of the PARACEST effect as well as to study the selectivity and strength of the interaction.

Characterization of outersphere complexes in solution is difficult because there are few spectroscopic methods for monitoring these indirect interactions. One promising method is high energy X-ray scattering of aqueous solutions of lanthanide(III) complexes.[28] In these studies, both innersphere and outersphere ligands are indentified. More commonly, NMR spectroscopy methods are used. For example, outersphere interactions have been monitored for Ln(III) complexes by using hyperfine shifted ^{13}C NMR ligand resonances.[29] Here we show that direct excitation lanthanide luminescence spectroscopy in conjunction with ^{1}H NMR spectroscopy enables us to determine the binding strength and to study the selectivity

of an unusual outersphere interaction between phosphate diester monoanions and lanthanide(III)-based PARACEST agents.

Experimental

Materials

[Ln(**S-THP**)]$(CF_3SO_3)_3$ complexes were prepared as reported previously.[26,30] MES buffer was used at pH 5.5 to 6.5 and HEPES buffer was used at pH 6.5 to 7.5 and EPPS buffer was used from pH 7.5 to 8.0. Diethyl phosphate (**DEP**), bis(4-nitrophenyl) phosphate (**BNPP**), 2',3'-cyclic AMP, O-(4-nitrophenylphosphoryl)choline (**NPPC**), phosphorothioic acid, O,O-diethylester (**DEPS**), ethyl methylphosphonate (**EMP**) were purchased from commercial sources and used without further purification.

CEST experiments

CEST experiments were acquired on an Inova-500 Spectrometer (11.7 T) at room temperature, B_1 = 800 Hz, (19 μT) with an irradiation time of 3 seconds. Measurements of the reduction of the percent water magnetization (M_z/M_o x 100) or saturation transfer (ST% = (1- M_z/M_o)x 100) had standard deviations of 1–2%. The CEST spectra were fit to modified Bloch equations with three exchangeable sites to obtain rate constants for exchange by using Matlab.[31] CEST imaging was performed on a phantom of 2×2 and 3×3 wells. A Varian 200 MHz horizontal bore NMR spectrometer was used for imaging. A standard spin-echo pulse sequence with presaturation was used to acquire the images. A 5 s presaturation pulse (B_1 = 11 μT) was employed with the TR = 10s, TE = 8.2 ms, matrix = 128 × 128, FOV = 35 mm x 35 mm, slice thickness = 5 mm, coronal slice. Images were collected by applying an on resonance saturation frequency at +21 ppm and an off resonance frequency at −21 ppm from the bulk water signal. The final CEST images were obtained by subtracting the −21 ppm (off-resonance) image from the +21 ppm image using the Image J (NIH) program.

Luminescence spectroscopy

Eu(III) excitation spectra and excited state lifetimes were obtained using a Spectra-Physics Quanta Ray PRO-270–10 Q-switched Nd:YAG pump laser (10 Hz, 60–70 mJ $pulse^{-1}$) and a MOPO SL for all luminescence measurements.[32] The $^7F_0 \rightarrow {}^5D_0$ transition of the Eu(III) ion was scanned between 578 and 581 nm while the $^5D_0 \rightarrow {}^7F_2$ emission band was monitored at 628 ± 27 nm using a band pass filter. Excitation spectra were fit by using the program Peak Fit 4.12 (Jandel). Binding constants determined from fits of luminescence data are reproducible to within ± 10%. Time resolved luminescence measurements were collected by using a digital Tektronix TDS 3034B oscilloscope. Data were fit to single exponential decays by using GraphPad Prism4. Solutions contained 10.0 mM Eu(**S-THP**)$^{3+}$, 20.0 mM EPPS buffer and 100.0 mM NaCl with zero to three equivalents of **DEP** at pH 8.0.

Data collection

A crystal (0.28 × 0.12 × 0.06 mm^3) was placed onto the tip of a 0.1 mm diameter glass capillary tube or fiber and mounted on a Bruker SMART APEX II CCD Platform diffractometer for a data collection at 100.0(1). A preliminary set of cell constants and an orientation matrix were calculated from reflections harvested from three orthogonal wedges of reciprocal space. The full data collection was carried out using MoKα radiation (graphite monochromator) with a frame time of 45 seconds and a detector distance of 4.98 cm. A randomly oriented region of reciprocal space was surveyed: six major sections of frames were collected with 0.50° steps in ω at six different φ settings and a detector position of −33° in 2ϑ. The intensity data were corrected for absorption (Sheldrick, G. M. SADABS, version 2008/1: University of Göttingen). Final cell constants were calculated from the xyz

centroids of 3833 strong reflections from the actual data collection after integration (SAINT, version 7.68A; Bruker AXS: Madison, WI, 2009). See Table 1 for additional crystal and refinement information.

Structure solution and refinement

The structure was solved using SIR97 and refined using SHELXL-97.33 The space group $P2_1$ was determined based on systematic absences and intensity statistics. A direct-methods solution was calculated which provided most non-hydrogen atoms from the E-map. Full-matrix least squares / difference Fourier cycles were performed which located the remaining non-hydrogen atoms. All non-hydrogen atoms were refined with anisotropic displacement parameters. The hydrogen atoms that participate in hydrogen bonding were either found from the difference Fourier map or placed in logical positions for hydrogen bonding. Once placed, their positions were fixed at O—H distances of 0.84 Å and they were refined relative to their bonded oxygen atoms. Their isotropic displacement parameters were also refined relative to equivalent isotropic displacement parameters of the respective oxygen atoms. All other hydrogen atoms were placed in ideal positions and refined as riding atoms with relative isotropic displacement parameters. The final full matrix least squares refinement converged to $R1 = 0.0763$ (F^2, $I > 2\sigma(I)$) and $wR2 = 0.1440$ (F^2, all data).

Results

CEST spectra

CEST spectra were recorded for Yb(**S-THP**)$^{3+}$ and Ce(**S-THP**)$^{3+}$ in solutions containing 20 mM buffer, 100 mM NaCl at near neutral pH. These spectra show the percent decrease in the water resonance plotted as a function of the frequency of the presaturation pulse (Figure 1). For both complexes, addition of a simple phosphate diester, diethylphosphate (**DEP**), enhances the PARACEST effect at near neutral pH, as observed previously for Eu(**S-THP**)$^{3+}$.24 Addition of **DEP** to Ce(**S-THP**)$^{3+}$ leads initially to an increase and sharpening of the CEST peak attributed to the alcohol protons of the complex. However, addition of more than one equivalent leads to a decrease in the CEST peak. Addition of **DEP** to solutions containing Yb(**S-THP**)$^{3+}$ leads to an increase in the CEST peak attributed to the alcohol protons of the complex. In contrast to the Ce(III) complex, the intensity of the PARACEST peak for the Yb(III) complex increases with concentration of **DEP** even at greater than one equivalent of **DEP**. A plot of the percent reduction in water magnetization, M_z/M_o of Yb(**S-THP**)$^{3+}$ as a function of **DEP** concentration at pH 7.0 is given in Figure S1. Data is fit to a 1:1 binding isotherm to give a K_d of 1.9 mM for the interaction of **DEP** with Yb(**S-THP**)$^{3+}$.

Further comparative CEST spectra were recorded on samples of Yb(**S-THP**)$^{3+}$ alone in buffer versus Yb(**S-THP**)$^{3+}$ plus two equivalents of **DEP**. These results indicate that CEST is larger for the sample containing **DEP** at all pH values from 5.5–7.5 but that the CEST difference is largest at pH 7 (Figure S2). This indicates that the optimum pH for CEST from Ln(**S-THP**)$^{3+}$ is below pH 3, consistent with reported PARACEST spectra,26 while the optimal pH for CEST from Ln(**S-THP**)$^{3+}$ plus **DEP** is near neutral pH. The PARACEST peak of Ln(**S-THP**)$^{3+}$ in the presence of two equivalents of **DEP** at pH 7.0 was nearly as intense at the physiological temperature of 37°C as at 22 °C (Figure S3).

Phantom images

To validate the observed CEST dependence of the Yb(**S-THP**)$^{3+}$ complex with respect to the pH, CEST imaging was done at 4.7 T for a 2×2 well phantom containing solutions of 5 mM Yb(**S-THP**)$^{3+}$ at different pH values as shown in Figure 2. The images were obtained by using a standard spin echo acquisition of the bulk water signal preceded by a

presaturation pulse on resonance (21 ppm) or off resonance (-21 ppm). The difference between these two images generates the CEST images of the phantoms. Imaging experiments in Figure 2i (left) are carried out on the complex in pure water which is the optimal condition for observation of the alcohol PARACEST effect for the complex alone. These individual wells show a pH dependent difference in CEST intensity with intensity decreasing from pH 4.5 to pH 7.0. At pH 7, there is no CEST seen which correlates with the result that is observed by using CEST spectroscopy.26 In contrast, phantom images as well as PARACEST spectra for Yb(**S-THP**)$^{3+}$ solutions in the presence of **DEP**, containing both buffer and 100 mM NaCl shows a reversal in the trend of their CEST effect as seen in (figure 2ii, right). Under these conditions, the most intense CEST contrast was observed for the solution at pH 7.0 in the presence of **DEP** and the least intense CEST effect was observed for the solution at pH 4.5 with **DEP**.

Luminescence, UV-vis and ^{1}H NMR Spectroscopy

To better understand the basis for **DEP** induced PARACEST changes, Ln(**S-THP**)$^{3+}$ complexes of **DEP** were studied by using ^{1}H NMR, UV-visible and luminescence spectroscopy. Luminescence spectroscopy of the Eu(**S-THP**)$^{3+}$ complex is especially useful in delineating the effect of **DEP** on the speciation of the Eu(III) complex in solution at different pH values. We monitor the $^7F_0 \rightarrow {}^5D_0$ Eu(III) transition which occurs between two non-degenerate states so that, barring overlap, each unique Eu(III) species in solution gives rise to a distinct excitation peak.34 The two peaks in the $^7F_0 \rightarrow {}^5D_0$ excitation spectrum of Eu(**S-THP**)$^{3+}$ have been assigned to ionized and non-ionized species as shown previously by the pH dependence of the excitation spectrum which correlates to pH-potentiometric titrations (Figure 3).35–36 The excitation peak at 577.7 nm is assigned to the ionized species (Eu(**S-THPD**)$(OH_2)^{2+}$) and the peak at 579.32 nm to the non-ionized form (Eu(**S-THP**)$OH_2)^{3+}$). The ionized species, (Eu(**S-THPD**)$(OH_2)^{2+}$), is proposed to be an alkoxide complex arising from deprotonation of an alcohol group, based on previous studies of reactivity of the complex in conjunction with luminescence properties (Scheme 1).35,37–39 For clarification of speciation in the following discussion, Eu(**S-THP**)$^{3+}$ designates the Eu(III) complex of **S-THP** for all species present in solution while Eu(**S-THPD**)$(OH_2)^{2+}$ designates only the ionized species and Eu(**S-THP**)$(OH_2)^{3+}$ designates only the non-ionized species.

Under conditions where the non-ionized complex is the major form, addition of **DEP** to Eu(**S-THP**)$^{3+}$ produces no change in the excitation spectrum, consistent with an outersphere complex ([Eu(**S-THP**)(OH_2)](**DEP**) as shown in Scheme 1.24 In addition, luminescence lifetime measurements in H_2O and D_2O are consistent with a single bound water for (Eu(**S-THP**)$(OH_2)^{3+}$) and ([Eu(**S-THP**)(OH_2)](**DEP**). Thus, as shown previously, **DEP** does not replace a water molecule and instead forms an innersphere complex with Eu(**S-THP**)$(OH_2)^{3+}$. However, addition of **DEP** to a solution of Eu(**S-THP**)$^{3+}$ at basic pH results in the disappearance of the excitation peak assigned to the ionized complex (577.7 nm) and a slight increase in the intensity of the excitation peak for the non-ionized species (Figure 3). This shows that outersphere **DEP** suppresses the formation of the ionized complex by interacting with the non-ionized complex (Scheme 1). A binding curve generated by monitoring the decrease in the excitation peak at 577.7 nm gives a K_d of 2.8 mM at pH 7.4, similar to that obtained by PARACEST titrations of **DEP** with the Yb(**S-THP**)$^{3+}$ complex (Figure S1).

Analogous to the luminescence data for the Eu(III) complex, the UV-vis spectrum of a solution of 5 mM Ce(**S-THP**)$^{3+}$ showing absorption bands arising from f→d orbital based transitions40 does not change in the presence of 1–5 equivalents of **DEP** at pH 6.5, conditions that show modulation of the CEST effect (compare Figure 1 and S4). This supports the formation of an outersphere Ce(**S-THP**)3 complex of **DEP**. In contrast, methylphosphate (**MP**) which forms an innersphere complex with Eu(**S-THP**)$^{3+}$ 24 also

appears to form an innersphere complexes with Ce(**S-THP**)$^{3+}$ as shown by changes in the UV-visible spectrum of Ce(**S-THP**)$^{3+}$ upon addition of **MP**. Consistent with innersphere complexation, the electronic transitions of Ce(**S-THP**)$^{3+}$ are perturbed upon binding of **MP** (Figure S4).

^{1}H NMR spectroscopy studies are also supportive of the formation of an outersphere **DEP** complex and with the conversion of the ionized species Ln(**S-THP**D)$(OH_2)^{2+}$ to the non-ionized species in the presence of **DEP**. As shown previously, addition of **DEP** to Eu(**S-THP**)$^{3+}$ leads to the appearance of a proton resonance assigned as the alcohol protons of the macrocyclic complex. In the absence of **DEP**, there is no visible alcohol proton resonance under similar conditions.24 This shows that the **DEP** interaction has a direct effect on alcohol proton exchange rate, as discussed further below. In addition to alcohol proton resonances, macrocyclic proton resonances are indicative of the nature of the complex. Under conditions where the non-ionized Eu(**S-THP**)$(OH_2)^{3+}$ is the major complex, the nonalcoholic macrocycle proton resonances do not change upon addition of **DEP** as would be expected for an outersphere interaction.24 In contrast, the ionized Yb(**S-THP**D)$(OH_2)^{2+}$ is the major complex in solution at pH 7.0 due to the low pK_a values of late Ln(**S-THP**)$^{3+}$ complexes.36,41 The ^{1}H NMR spectrum of Yb(**S-THP**)$^{3+}$ changes dramatically at high and low pH because the ionized and non-ionized species have distinct hyperfine shifted macrocycle proton resonances (Figure S5). Addition of **DEP** to a solution of the Yb(**S-THP**)$^{3+}$ complex at pH 7.0 shifts the macrocycle ^{1}H resonances of the complex from those of the ionized complex, Yb(**S-THPD**)$(OH_2)^{2+}$, to match those of Yb(**S-THP**)$(OH_2)^{3+}$ (Figure S5). This suggests that outersphere binding of **DEP** to the Yb(**S-THP**)$(OH_2)^{3+}$ complex inhibits its ionization (Scheme 1). Thus ^{1}H NMR spectroscopy data for Eu(**S-THP**)$^{3+}$ and Yb(**S-THP**)$^{3+}$ supports the luminescence spectroscopy studies of **DEP** induced speciation changes of the Eu(**S-THP**)$^{3+}$ complex.

To explore the specificity of the outersphere interaction, several different phosphate esters were studied as agents to activate Yb(**S-THP**)$^{3+}$ and Eu(**S-THP**)$^{3+}$ PARACEST agents. Biologically relevant esters include **NPPC**, a phospholipid analog, and cyclic-3'-5'-**AMP**. Phosphate esters not found in biological systems, **BNPP, DEPS** and **EMP** were studied to better understand the nature of the outersphere interaction. Remarkably, only **DEP** and **BNPP** affect the PARACEST spectrum of Yb(**S-THP**)$^{3+}$ or Eu(**S-THP**)$^{3+}$ upon addition of 1–2 equivalents of phosphate ester, the solubility limit for the biologically relevant esters or up to 20-equivalents for **DEPS** and **EMP** with Yb(**S-THP**)$^{3+}$ (Figure S6–S7). **BNPP** binds more weakly than **DEP** as shown by the relatively small effect of one equivalent of **BNPP** on the PARACEST spectrum of Eu(**S-THP**)$^{3+}$ compared to **DEP** at pH 6.5 (Figure S7a). Similarly, **BNPP** gives the same PARACEST increase with Yb(**S-THP**)$^{3+}$ as does **DEP** at at pH 5.5 but does not have an effect on Yb(**S-THP**)$^{3+}$ PARACEST at pH 7.0 (compare Figure S7a and S7b). Furthermore, unlike **DEP, BNPP** has little effect on the luminescence excitation peak of Eu(**S-THP**D)$(OH_2)^{2+}$ (pH 7.5) at concentrations of 5 mM, the upper limit for solubility (data not shown). This suggests that **BNPP** does not bind strongly enough to Ln(**S-THP**)$(OH_2)^{3+}$ to suppress ionization and activate PARACEST at neutral pH under conditions favorable for ionization, but does bind sufficiently strongly at acidic pH values where ionization is not an important competing process. Thus **BNPP** should give rise to a distinct pH dependence for the PARACEST spectrum of Yb(**S-THP**)$^{3+}$ because it activates CEST only at more acidic pH values.

Luminescence titrations by monitoring the $^{7}F_0 \rightarrow {}^{5}D_0$ Eu(III) excitation peak show that **NPPC**, cyclic-3'-5'-**AMP, DEPS** and **EMP** do not change the excitation spectrum of the Eu(**S-THP**)$^{3+}$ complex at pH 7.5 (Figure S8) in contrast to observations for **DEP** (Figure 3). The weaker binding of these phosphate diesters to Eu(**S-THP**)$(OH_2)^{3+}$ in comparison to **DEP** provides a rationale for their inability to activate PARACEST.

Crystal Structure

To further characterize the outersphere interaction of Ln(**S-THP**)$^{3+}$ complexes with phosphate esters, a crystal structure of [Eu(**S-THP**)(OH_2)](**BNPP**)$_2$(CF_3SO_3) · 2H_2O · iPrOH was obtained (Figure 4). The unit cell contains two crystallographically independent Eu(III) complexes that have the same macrocyclic complex stereochemistry. The coordination sphere of the complex cation, [Eu(**S-THP**)(OH_2)]$^{3+}$ has a twisted square prismatic geometry with a capping water molecule. Consistent with this geometrical assignment,42 the twist angle between the two square planes of the antiprism consisting of the four basal nitrogens and the four alcohol oxygens is 22°. All Eu-O or Eu-N distances are similar to those observed previously in a crystal structure of the complex cation lacking the phosphate diester which contained two diastereomeric complex cations (Eu(**RRRS-THP**)(H_2O)](CF_3SO_3)$_3$ and (Eu(**SSSR-THP**)(H_2O)](CF_3SO_3)$_3$.30 In this earlier crystal structure, complex cations with both the capped twisted square antiprismatic geometry and the capped square antiprismatic isomer were found. In the work here only a single diastereomer is observed for the simpler case that has **SSSS-THP** (**S-THP**) as the macrocyclic ligand. The outersphere interactions include an extensive hydrogen bonding network between the macrocycle alcohol or water ligand protons and the two outersphere phosphate diesters. For both **BNPP** molecules, a single oxygen of each of the phosphate esters is within hydrogen bonding distance of the alcohol proton and one of the bound water protons of the complex. The second phosphate oxygen of each **BNPP** is involved in hydrogen bonding to two outersphere water molecules. The remaining two alcohol protons of the **S-THP** macrocycle are within hydrogen bonding distance of the 2-propanol and one of the second sphere water molecules. The triflate counterion is not involved in the hydrogen bonding network.

Discussion

Previous studies indentified the alcohol protons of the Ln(**S-THP**)$^{3+}$ complexes as the exchangeable protons that give rise to the PARACEST spectrum. This assignment was based on the identification of the alcohol proton and bound water resonances in acetonitrile and acetonitrile/water mixtures and comparison of the chemical shift of the alcohol resonances with the CEST spectrum.24,27,43 This assignment is also supported by the very rapid exchange rate constant for the water ligand in Ln(**S-THP**)$^{3+}$ that makes it unlikely that the water ligand will contribute to the CEST spectrum.44 The large pH dependence of the PARACEST effect of these complexes is attributed, in part, to the ionization of the Ln(**S-THP**)$^{3+}$ complexes to form a new species.30 The non-ionized complex contains a single bound water (Ln(**S-THP**)(OH_2)$^{3+}$) and the ionized complex most likely involves deprotonation of the alcohol to give (Ln(**S-THP**D)(OH_2)$^{2+}$) (Scheme 1).35 Reported pK_a values for La(**S-THP**)$^{3+}$, Eu(**S-THP**)$^{3+}$ and Yb(**S-THP**)$^{3+}$, Lu(**S-THP**)$^{3+}$ are 8.5, 7.5, 6.4 and 6.5, respectively.36,41 The pK_a value for Ce(**S-THP**)$^{3+}$ is assumed to be close to that of the La(III) complex, in line with the monotonic decrease of pK_a values across the lanthanide series. Thus, early and mid-lanthanides such as Eu(**S-THP**)$^{3+}$ and Ce(**S-THP**)$^{3+}$ have the non-ionized complex as the dominant species in solution at acidic pH. It is the non-ionized complex which gives rise to a PARACEST effect; no PARACEST is observed at pH values where the ionized species is dominant. Similarly, the PARACEST effect for Yb(**S-THP**)$^{3+}$ is strongest at pH values where the non-ionized form is the major species in solution, in this case at pH 3.43

Proton exchange rate constants as determined by fitting PARACEST spectra31 show that **DEP** binding optimizes the rate constants for proton exchange between the lanthanide complex and bulk water. In the absence of **DEP** at pH 7.0, the proton exchange rate constant for Yb(**S-THP**)$^{3+}$ is 54 s^{-1}. This rate constant increases to 300 s^{-1} in the presence of **DEP** at pH 7.0. The higher rate constant for proton exchange leads to more effective PARACEST for the Yb(III) complex as predicted by the relationship between saturation transfer and

mobile proton exchange rate constants.45 Notably, the rate constant for proton exchange in the presence of **DEP** is similar to that of the complex under acidic conditions (pH 3.1) where the non-ionized complex dominates (370 s^{-1}). Based on these observations and the ^{1}H NMR studies of the complex speciation, we assign [Yb(**S-THP**)(OH_2)](**DEP**) as the species which produces the PARACEST spectrum at neutral pH. An alternative is a complex with two outersphere **DEP** molecules, based on the presence of two DEP molecules in the crystal structure. However, binding isotherms are most consistent with a single molecule of **DEP** interacting with Ln(**S-THP**)$^{3+}$.

Ce(**S-THP**)$^{3+}$ rate constants for alcohol proton exchange are 1040 s^{-1} and 430s^{-1} in the absence and presence of 1 equivalent of **DEP**, respectively. Here the role of **DEP** is to decrease rate constants that are too large to obtain a strong PARACEST alcohol peak. For Ce(**S-THP**)$^{3+}$ and Eu(**S-THP**)$^{3+}$ the slow exchange limit is almost exceeded at near neutral pH as a result of the small separation between the alcohol proton resonances and that of bulk water.26 Addition of an equivalent of **DEP** serves to sharpen the PARACEST alcohol peak by lowering the rate constant for exchange.24 For Ce(**S-THP**)$^{3+}$ addition of a two-fold excess of **DEP** decreases the CEST effect, a complication not observed for the Eu(III) or Yb(III) complex.

We propose that **DEP** interacts with Ln(**S-THP**)(OH_2)$^{3+}$ through the alcoholic and water ligand protons of the complexes as shown in Scheme 1. This second coordination sphere binding mode is consistent with the change in proton exchange rate constants of Ln(**S-THP**)$^{3+}$ upon addition of **DEP** and with the suppression of the formation of the ionized species through the formation of a specific outersphere interaction. Examination of the crystal structure suggests that an extensive hydrogen bonding network that includes the phosphate ester oxygens, the alcohol groups and both inner and outersphere water ligands may be important in these interactions. The involvement of both the macrocyclic alcohol protons and the water ligand protons in interaction with the phosphate diester raises the question of which protons in the complex give rise to the CEST peak for [Ln(**S-THP**)(OH_2)](**DEP**). We propose that it is the alcohol protons in the complex with **DEP** that give rise to the CEST effect based on the similarity of the chemical shift of the protons that give rise to the CEST effect for [Ln(**S-THP**)(OH_2)](**DEP**) to that of the alcohol protons in [Ln(**S-THP**)(OH_2)]$^{3+}$.24،27،43

The outersphere interaction requires two terminal oxygen donors and two identical ester groups on the phosphate diester. Curiously, this interaction is not highly selective for simple uncharged ester groups because both **BNPP** and **DEP** activate PARACEST. However, phosphate diesters which do not have identical ester groups do not activate PARACEST. For example, **NPPC** does not bind to Eu(**S-THP**)$^{3+}$ or activate PARACEST. The weaker interaction of **NPPC** with the cationic Ln(III) complexes is attributed to the overall neutral charge of this phosphate ester. In cyclic phosphate diesters, the two oxygen atoms have distinctly different electronic charge distributions 46 which may be important in preventing the formation of the outersphere complex. This is supported by the most surprising result, that two compounds even more structurally similar to **DEP**, such as **DEP**S and **EMP**, do not affect the PARACEST spectra of Ln(**S-THP**)$^{3+}$ even at a 20-fold excess of phosphate ester. That such subtle changes in the phosphate groups reduce interaction with Ln(**S-THP**)$^{3+}$ suggests that electronic charge distribution on the terminal and bridging oxygens is an important factor in the formation of a specific outersphere interaction. That the simple **DEP** monoanion forms a relatively strong and specific outersphere complex (K_d = 2–3 mM) under conditions of high salt concentration is quite remarkable.

Conclusions

In summary, phosphate diesters (**PDE**) that modulate the PARACEST spectrum of Ln(**S-THP**)$^{3+}$ interact with the non-ionized complex to form [Ln(**S-THP**)(OH_2)](**PDE**) as supported by luminescence spectroscopy of the Eu(III) complex, UV-vis spectroscopy of the Ce(III) complex, and ^{1}H NMR spectroscopy of the Yb(III) and Eu(III) complexes. This outersphere complex has exchange rate constants that are more suitable for PARACEST at neutral pH than those of the complex under these conditions in the absence of **DEP**. This interaction serves to switch on the alcohol PARACEST peak of the complexes at neutral pH in buffered solutions containing 100 mM NaCl. An interesting feature of this work is the selective formation of an outersphere complex with symmetrical phosphate diesters. The complex cation in the structure shown here, [Eu(***S*-THP**)(OH_2)](**BNPP**)$_2$(CF_3SO_3) · $2H_2O$ · iPrOH, has two outersphere phosphate diesters that participate in an extensive hydrogen bonding network with the alcohol protons and water ligand of the macrocyclic complex.

This work shows that outersphere interactions of Ln(III) complexes may be useful for the modulation of PARACEST properties even in systems that lack designed binding sites for inducing a specific response to a desired anionic ligand or cation. Efforts are underway to further probe the specificity of this interaction and to determine whether enhanced binding pockets,47 will modulate the selectivity and strength of binding for the detection of phosphate ester metabolites that are biomarkers for disease.48–49

Supplementary Material

Refer to Web version on PubMed Central for supplementary material.

Acknowledgments

This work was supported in part by grants from the National Institutes of Health (EB-04609 to J.R.M., RR-02584 and CA-115531 to A.D.S.) and from the National Science Foundation for a major instrumentation award (CHE-0321058 to J.R.M.) to build the MOPO laser system. J.R. M. thanks Jean-Marc Escudier of Université Paul Sabatier for helpful discussions. We thank William W. Brennessel of the X-ray Crystallographic Facility, Department of Chemistry, University of Rochester for solving the crystal structure presented here.

References

1. Yoo B, Pagel MD. Front. Biosci. 2008; 13:1733. [PubMed: 17981664]
2. Sherry AD, Woods M. Annu. Rev. Biomed. Eng. 2008; 10:391. [PubMed: 18647117]
3. Major JL, Meade TJ. Acc. Chem. Res. 2009; 42:893. [PubMed: 19537782]
4. Aime S, Barge A, Castelli DD, Fedeli F, Mortillaro A, Nielsen FU, Terreno E. Magn. Reson. Med. 2002; 47:639. [PubMed: 11948724]
5. Ren J, Trokowski R, Zhang S, Malloy CR, Sherry AD. Magn. Reson. Med. 2008; 60:1047. [PubMed: 18958853]
6. van Zijl PCM, Jones CK, Ren J, Malloy CR, Sherry AD. Proc. Natl. Acad. Sci. U. S. A. 2007; 104:4359. [PubMed: 17360529]
7. Woods M, Zhang S, Von Howard E, Sherry AD. Chem. Eur. J. 2003; 9:4634.
8. Major JL, Parigi G, Luchinat C, Meade TJ. Proc. Natl. Acad. Sci. U. S. A. 2007; 104:13881. [PubMed: 17724345]
9. Que EL, Chang CJ. J. Am. Chem. Soc. 2006; 128:15942. [PubMed: 17165700]
10. Zhang, X-a; Lovejoy, KS.; Jasanoff, A.; Lippard, SJ. Proc. Natl. Acad. Sci. U. S. A. 2007; 104:10780. [PubMed: 17578918]
11. Ali MM, Woods M, Suh EH, Kovacs Z, Tircso G, Zhao P, Kodibagkar VD, Sherry AD. J. Biol. Inorg. Chem. 2007; 12:855. [PubMed: 17534672]

12. Yoo B, Raam MS, Rosenblum RM, Pagel MD. Contrast Media Mol. Imaging. 2007; 2:189. [PubMed: 17712869]
13. Chauvin T, Durand P, Bernier M, Meudal H, Doan B-T, Noury F, Badet B, Beloeil J-C, Toth E. Angew. Chemie, Int. Ed. 2008; 47:4370.
14. Caravan P. Acc. Chem. Res. 2009; 42:851. [PubMed: 19222207]
15. Thompson AL, Parker D, Fulton DA, Howard JAK, Pandya SU, Puschmann H, Senanayake K, Stenson PA, Badari A, Botta M, Avedano S, Aime S. Dalton Trans. 2006:5605. [PubMed: 17225897]
16. Yerly F, Borel A, Helm L, Merbach AE. Chem. Eur. J. 2003; 9:5468.
17. Kotkova Z, Pereira GA, Djanashvili K, Kotek J, Rudovsky J, Hermann P, Vander Elst L, Muller RN, Geraldes CFGC, Lukes I, Peters JA. Eur. J. Inorg. Chem. 2009:119.
18. Barge A, Botta M, Parker D, Puschmann H. Chem. Commun. 2003:1386.
19. De Leon-Rodriguez LM, Lubag AJM, Malloy CR, Martinez GV, Gillies RJ, Sherry AD. Acc. Chem. Res. 2009; 42:948. [PubMed: 19265438]
20. Woods M, Woessner DE, Sherry AD. Chem. Soc. Rev. 2006; 35:500. [PubMed: 16729144]
21. Aime S, Delli Castelli D, Geninatti Crich S, Gianolio E, Terreno E. Acc. Chem. Res. 2009; 42:822. [PubMed: 19534516]
22. Esqueda AC, Lopez JA, Andreu-de-Riquer G, Alvarado-Monzon JC, Ratnakar J, Lubag AJM, Sherry AD, De Leon-Rodriguez LM. J. Am. Chem. Soc. 2009; 131:11387. [PubMed: 19630391]
23. Trokowski R, Zhang S, Sherry AD. Bioconjugate Chem. 2004; 15:1431.
24. Huang C-H, Morrow JR. J. Am. Chem. Soc. 2009; 131:4206. [PubMed: 19317496]
25. Aime S, Delli Castelli D, Fedeli F, Terreno E. J. Am. Chem. Soc. 2002; 124:9364. [PubMed: 12167018]
26. Huang C-H, Morrow JR. Inorg. Chem. 2009; 48:7237. [PubMed: 19722692]
27. Woods M, Woessner DE, Zhao PY, Pasha A, Yang MY, Huang CH, Vasalitiy O, Morrow JR, Sherry AD. J. Am. Chem. Soc. 2006; 128:10155. [PubMed: 16881645]
28. Soderholm L, Skanthakumar S, Wilson RE. J. Phys. Chem A. 2009; 113:6391. [PubMed: 19432479]
29. Corsi DM, van Bekkum H, Peters JA. Inorg. Chem. 2000; 39:4802. [PubMed: 11196957]
30. Chin KOA, Morrow JR, Lake CH, Churchill MR. Inorg. Chem. 1994; 33:656.
31. Woessner DE, Zhang S, Merritt ME, Sherry AD. Magn. Reson. Med. 2005; 53:790. [PubMed: 15799055]
32. Andolina CM, Holthoff WG, Page PM, Mathews RA, Morrow JR, Bright FV. Appl. Spectrosc. 2009; 63:483. [PubMed: 19470203]
33. Sheldrick GM. Acta Crystallogr., Sect. A: Found. Crystallogr. 2008:112.
34. Horrocks WD Jr, Sudnick DR. J. Am. Chem. Soc. 1979; 101:334.
35. Chappell LL, Voss DA, Horrocks WD, Morrow JR. Inorg. Chem. 1998; 37:3989. [PubMed: 11670514]
36. Chin KOA, Morrow JR. Inorg. Chem. 1994; 33:5036.
37. Baker BF, Khalili H, Wei N, Morrow JR. J. Am. Chem. Soc. 1997; 119:8749.
38. Epstein DM, Chappell LL, Khalili H, Supkowski RM, Horrocks WD Jr, Morrow JR. Inorg. Chem. 2000; 39:2130. [PubMed: 12526524]
39. Morrow JR, Aures K, Epstein D. J. Chem. Soc., Chem. Commun. 1995:2431.
40. Frey ST, Horrocks WD Jr. Inorg. Chem. 1991; 30:1073.
41. Lelli M, Pintacuda G, Cuzzola A, Di Bari L. Chirality. 2005; 17:201. [PubMed: 15828032]
42. Benetollo F, Bombieri G, Calabi L, Aime S, Botta M. Inorg. Chem. 2003; 42:148. [PubMed: 12513089]
43. Huang C-H, Morrow JR. Inorg. Chem. 2009; 48:7237. [PubMed: 19722692]
44. Corsi DM, Vander Elst L, Muller RN, van Bekkum H, Peters JA. Chem. Eur. J. 2001; 7:1383.
45. Zhang S, Merritt M, Woessner DE, Lenkinski RE, Sherry AD. Acc. Chem. Res. 2003; 36:783. [PubMed: 14567712]

46. Gerlt JA, Demou PC, Mehdi SJ. Am. Chem. Soc. 1982; 104:2848.

47. Damsyik A, Lincoln SF, Wainwright KP. Inorg. Chem. 2006; 45:9834. [PubMed: 17112281]

48. Glunde K, Ackerstaff E, Mori N, Jacobs MA, Bhujwalla ZM. Molecular Pharmaceutics. 2006; 3:496. [PubMed: 17009848]

49. Stanley JA, Kipp H, Greisenegger E, MacMaster FP, Panchalingam K, Pettegrew JW, Keshavan MS, Bukstein OG. Psychiatry Research : Neuroimaging. 2006; 148:217.

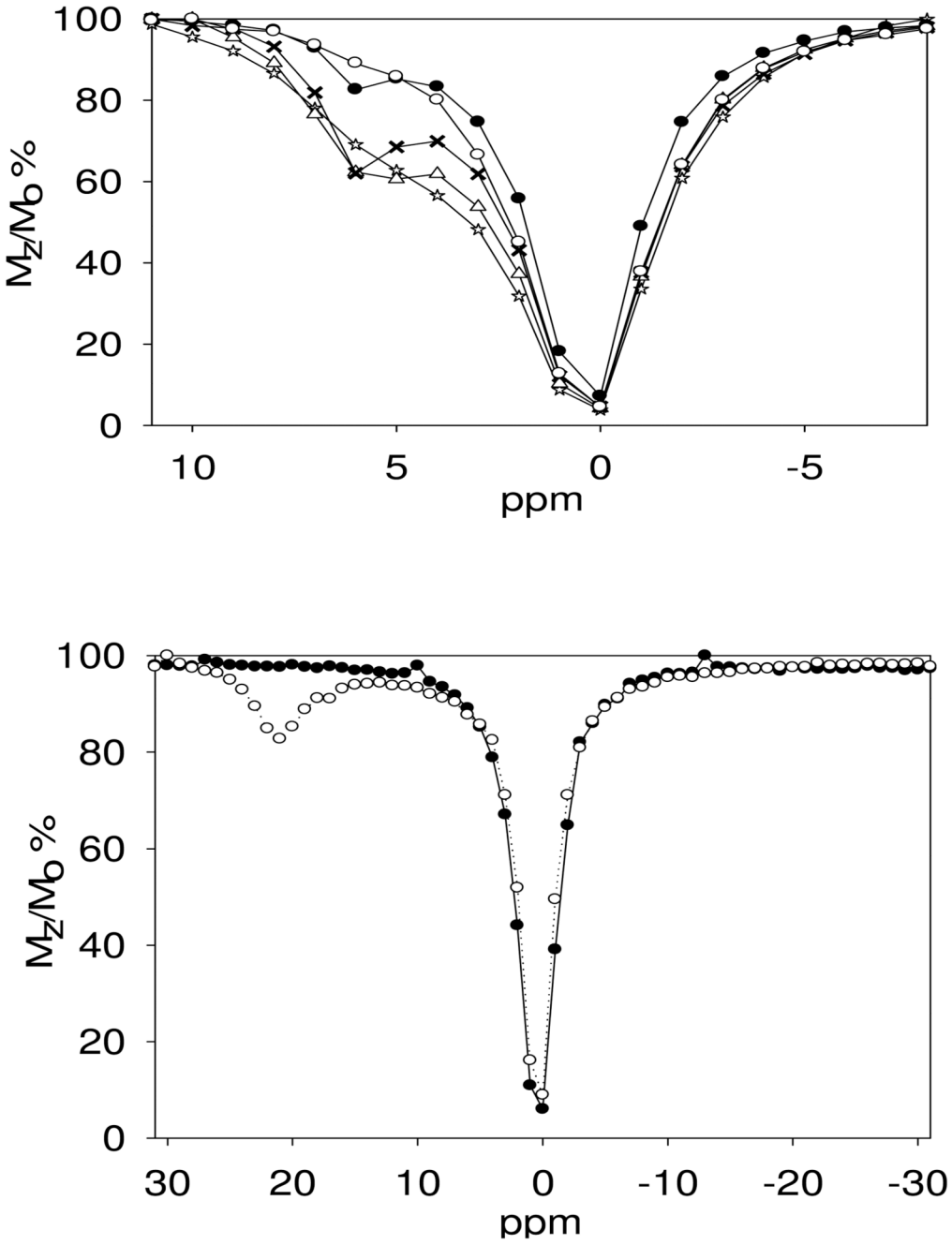

Figure 1.

Top: PARACEST spectra of 10.0 mM Ce(**S-THP**)$^{3+}$ with addition of diethylphosphate (**DEP**) at pH 6.5, 100 mM NaCl, 20 mM Mes buffer. (☆) 0.0 mM, (Δ) 5.0 mM, (X) 10.0 mM, (○) 15.0 mM, (●) 20.0 mM. bottom: PARACEST spectra of 5 mM Yb(**S-THP**)$^{3+}$, 20 mM buffer and 100 mM NaCl at pH 7.0 with (○) and without (●)addition of 10 mM **DEP**. Presaturation pulse (B_1) was 800 Hz for 3 s at 22°C.

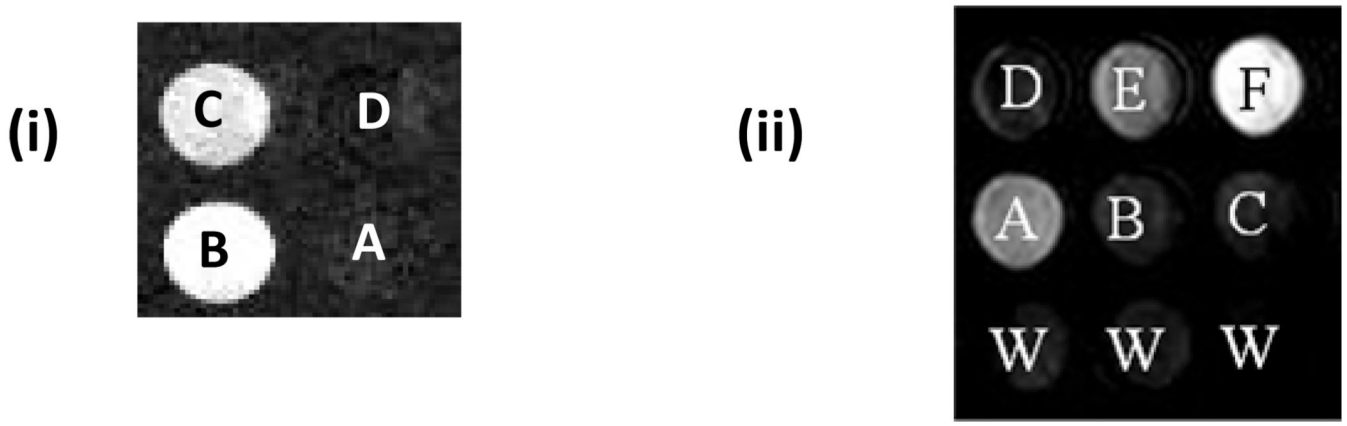

Figure 2.

i) CEST images at 4.7 T of 5.00 mM Yb(**S-THP**)$^{3+}$ in pure water, 25 °C, at different pH values: (A) pure water as a control; (B) pH 4.5; (C) pH 5.5; (D) pH 7.0, and ii) Lower row from left to right: water as control (W). Middle row from left to right: 5.00 mM Yb(**S-THP**)$^{3+}$, 20.0 mM buffer and 100 mM NaCl at pH 4.6 (A), 5.5 (B) and 7.0 (C). Upper row form left to right: Addition of 10.0 mM **DEP** to 5.00 mM Yb(**S-THP**)$^{3+}$, 20.0 mM buffer and 100 mM NaCl at pH 4.6 (D), 5.5 (E) and 7.0 (F).

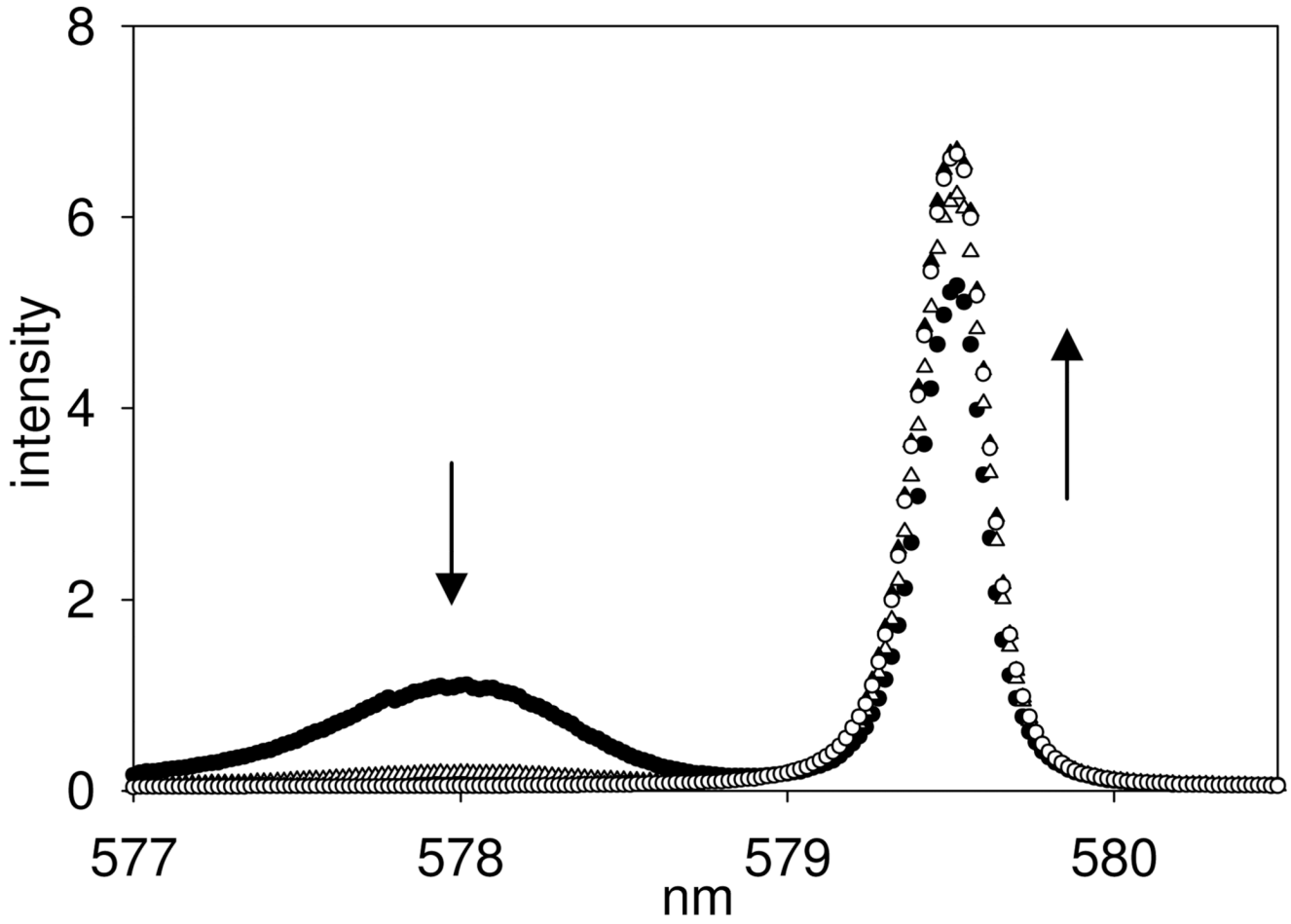

Figure 3.

$^7F_0 \rightarrow {}^5D_0$ excitation spectra ($^5D_0 \rightarrow {}^7F_2$ emission) of 10.0 mM Eu(**S-THP**)$^{3+}$, 20.0 mM buffer and 100.0 mM NaCl with ^{DEP} (●) 0 mM, (△) 10 mM, (▲) 20.0 mM, (○) 30 mM at pH 8.0, 22°C.

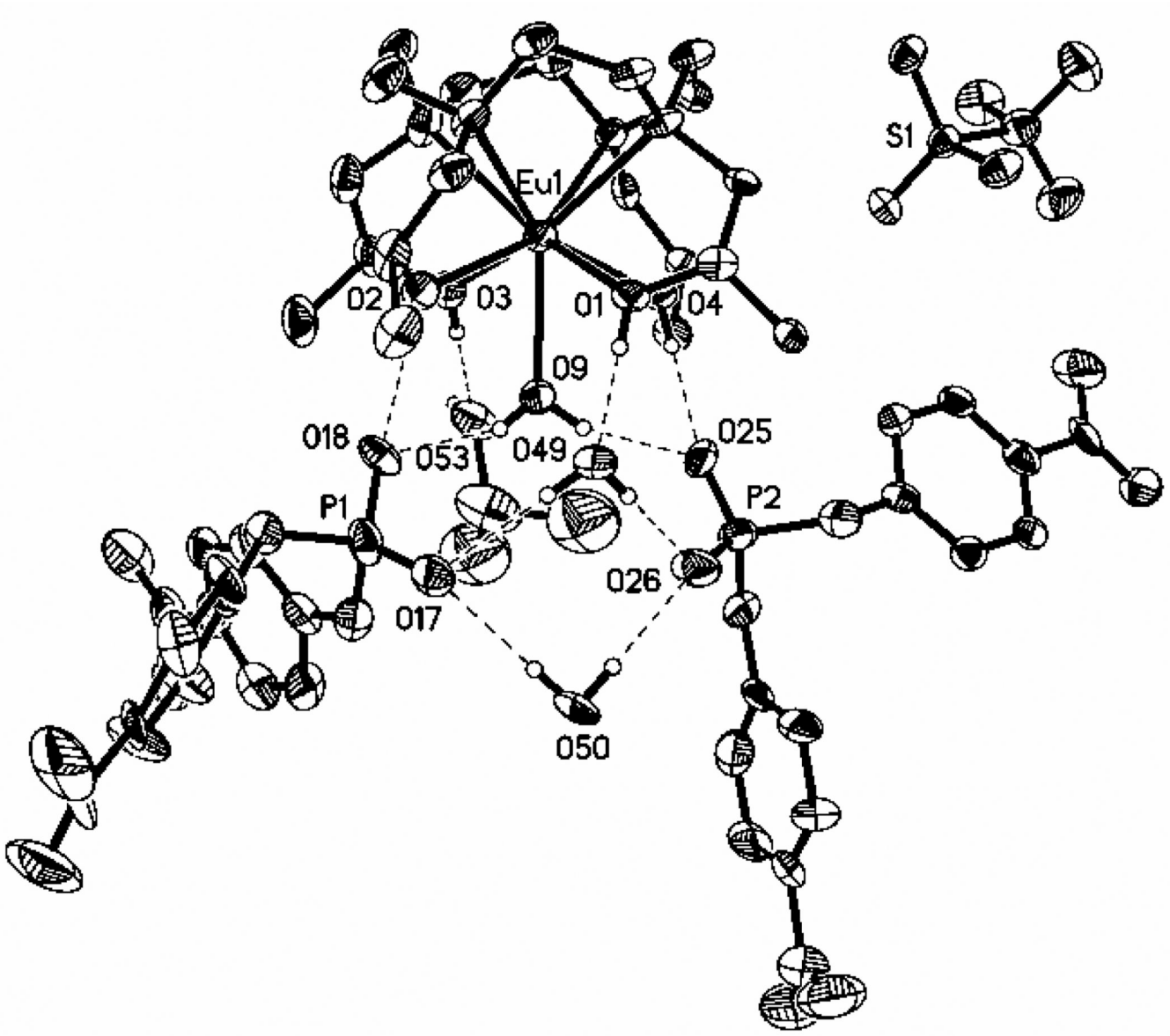

Figure 4.

Ortep diagram (50% ellipsoids) of [Eu(*S*-THP)(OH_2)][$(O_2NPhO)_2PO_2]_2$[CF_3SO_3] · 2H_2O · iPrOH. Selected bon lengths (Å): Eu(1)-O(3), 2.373(6); Eu(1)-O(1), 2.386(5); Eu(1)-O(2), 2.422(5); Eu(1)-O(4), 2.423(4); Eu(1)-O(9,)2.450(5); Eu(1)-N(1), 2.711(7); Eu(1)-N(2), 2.676(6); Eu(1)-N(3), 2.671(7); Eu(1)-N(4), 2.612(6). Bond angles (deg): O(3)-Eu(1)-O(1), 137.79(18); O(3)-Eu(1)-O(2), 82.49(19); O(3)-Eu(1)-O(9), 66.52(19); O(1)-Eu(1)-O(9), 71.48(18); O(1)-Eu(1)-N(1), 63.13(18).

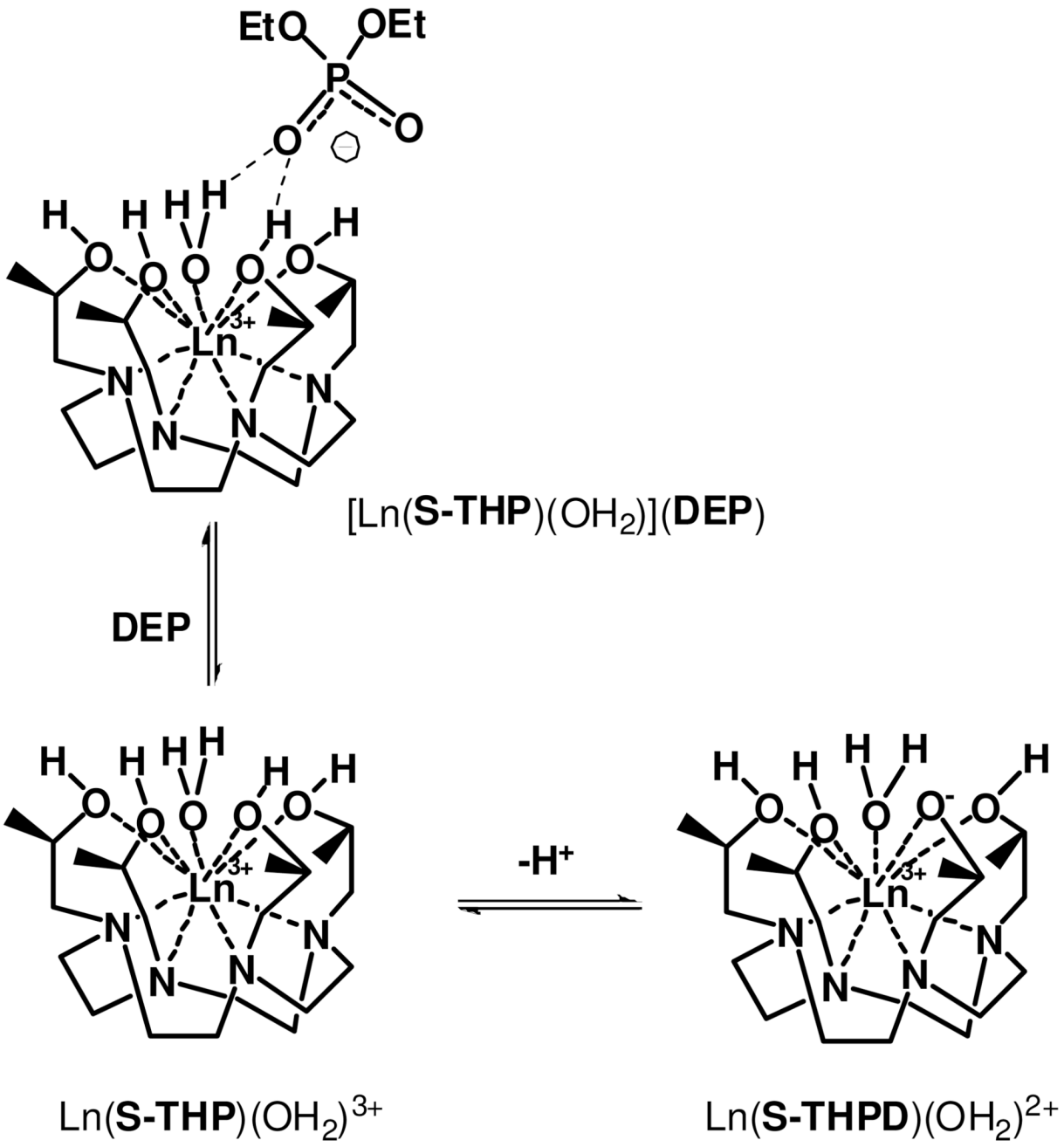

Chart 1.

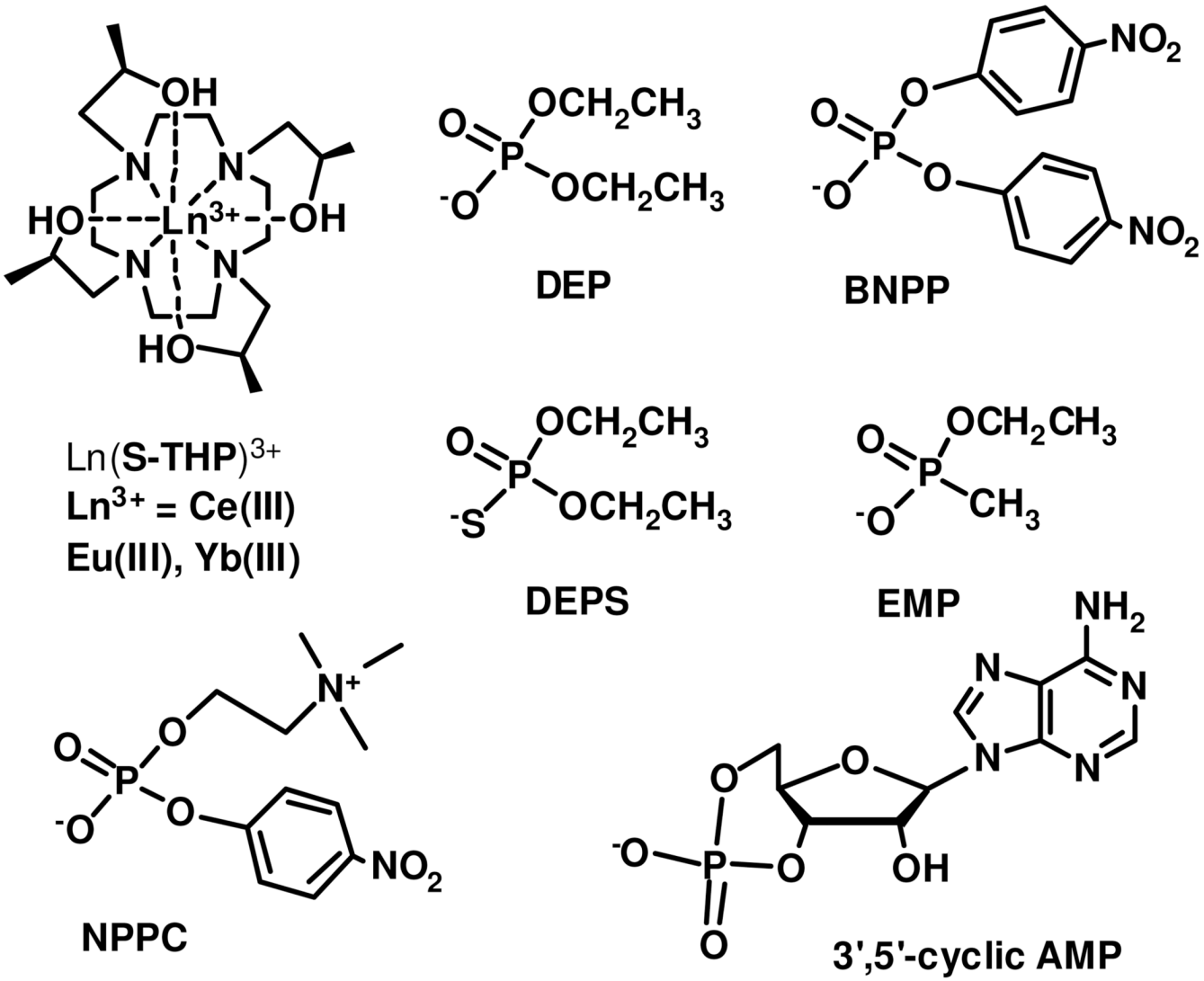

Scheme 1.

Table 1

Crystal data and structure refinement for $[Eu(S\text{-}THP)(OH_2)][(O_2NPhO)_2PO_2]_2[CF_3SO_3] \cdot 2H_2O \cdot iPrOH$

Empirical formula	C48 H74 Eu F3 N8 O27 P2 S	
Formula weight	1498.11	
Temperature	100.0(1) K	
Wavelength	0.71073 Å	
Crystal system	Monoclinic	
Space group	$P2_1$	
Unit cell dimensions	a = 25.491(5) Å	α = 90°
	b = 9.8057(18) Å	β = 112.122(3)°
	c = 27.192(5) Å	γ = 90°
Volume	6296(2) $Å^3$	
Z	4	
Density (calculated)	3 1.580 Mg/m^3	
Absorption coefficient	1.178 mm^{-1}	
F(000)	3080	
Crystal color, morphology	colorless, plate	
Crystal size	0.28 × 0.12 × 0.06 mm^3	
Theta range for data collection	1.39 to 29.57°	
Index ranges	$-35 \leq h \leq 35$, $-13 \leq k \leq 13$, $-37 \leq l \leq 37$	
Reflections collected	136522	
Independent reflections	35308 [R(int) = 0.0803]	
Observed reflections	29118	
Completeness to theta = 29.57°	99.9%	
Absorption correction	Multi-scan	
Max. and min. transmission	0.9327 and 0.7339	
Refinement method	Full-matrix least-squares on F^2	
Data / restraints / parameters	35308 / 93 / 1635	
Goodness-of-fit on F^2	1.161	
Final R indices [I>2sigma(I)]	$R1$ = 0.0763, $wR2$ = 0.1382	
R indices (all data)	$R1$ = 0.0932, $wR2$ = 0.1440	
Absolute structure parameter	0.042(9)	
Largest diff. peak and hole	1.931 and −3.732 e.$Å^{-3}$	